ACS APPLIED MATERIALS & INTERFACES

www.acsami.org

Research Article

Light-Triggered Bioorthogonal Nanozyme Hydrogels for Prodrug Activation and Treatment of Bacterial Biofilms

Published as part of ACS Applied Materials & Interfaces special issue "Nanozymes: Design, Mechanisms, and Applications".

Aarohi Gupta, Muhammad Aamir Hassan, William Ndugire, Jungmi Park, Sadaf Noor, Harini Nagaraj, Soham Chakraborty, and Vincent M. Rotello*

Cite This: ACS Appl. Mater. Interfaces 2025, 17, 26361−26370

Read Online

ACCESS | Metrics & More | Article Recommendations | Supporting Information

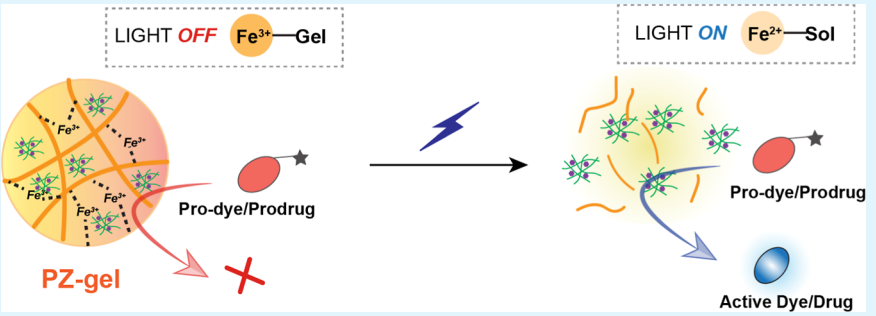

ABSTRACT: Bioorthogonal nanozymes offer in situ activation of pro-dyes and prodrugs using abiotic chemical transformations. Bacterial infections, especially biofilm-associated infections, are extremely difficult to treat due to obstacles such as poor antibiotic penetration and the rising threat of antibiotic resistance. Spatiotemporal control of bioorthogonal catalysis provides a strategy for "on-demand" generation of therapeutics, effectively localizing therapeutic action and minimizing side effects. Here, we present the fabrication of visible-light-responsive alginate hydrogel beads embedded with bioorthogonal polyzymes (PZs). Exposure to a 405 nm light induces the reduction of Fe(III) to Fe(II), triggering the dissolution of the **PZ-gel** beads with concomitant release and activation of the polyzyme. This approach enabled the selective activation of a prodrug of Linezolid, a last-in-line antibiotic for Gram-positive bacterial infections, enabling the targeted eradication of multidrug-resistant*Staphylococcus aureus* biofilms. Overall, the use of alginate biomaterial along with noninvasive visible light offers a nontoxic platform for spatiotemporal release of antibiotics through bioorthogonal activation.

KEYWORDS: *bioorthogonal catalysis, spatiotemporal, light activation, bacterial biofilms, alginate hydrogels*

INTRODUCTION

Bioorthogonal chemistry enables synthetic reactions that do not interfere with natural biological processes.[1,2] Bioorthogonal catalysis has been enabled through the use of abiotic transition-metal catalysts (TMCs) in living cells and organisms.[3,4] TMCs incorporating Pd,[5] Ru,[6] and Au[7] are particularly well-suited for bioorthogonal catalysis, facilitating selective reactions that are independent of biochemical pathways. This orthogonality allows researchers to introduce and control chemical processes in living cells or tissues without disrupting their normal functions. Prodrug and pro-dye substrates can be designed to be selectively cleaved in the presence of TMCs.[3,4] This ability of TMCs makes possible the *in situ* activation of prodrugs at targeted sites (e.g., tumors or infectious wounds),[8] uncaging pro-dyes for imaging and chemical labeling of biomolecules.[9] Such localized production of bioactive agents enables targeted therapies with minimal side effects and offers powerful tools for imaging, drug delivery, and biological research.[10−12] However, challenges related to solubility, biocompatibility, and stability make the direct use of TMCs in physiological settings difficult.[3,4,13,14] These issues can be mitigated by encapsulating TMCs within nanoparticles (nanozymes)[15,16] and polymers (polyzymes, PZ)[17,18] that provide aqueous solubility and stability while preserving catalytic activity.[3,11] This approach creates bioorthogonal nanocatalysts that utilize synthetic nanomaterials and polymers to stabilize TMCs. Additionally,

Received: January 29, 2025
Revised: April 14, 2025
Accepted: April 15, 2025
Published: April 24, 2025

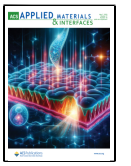

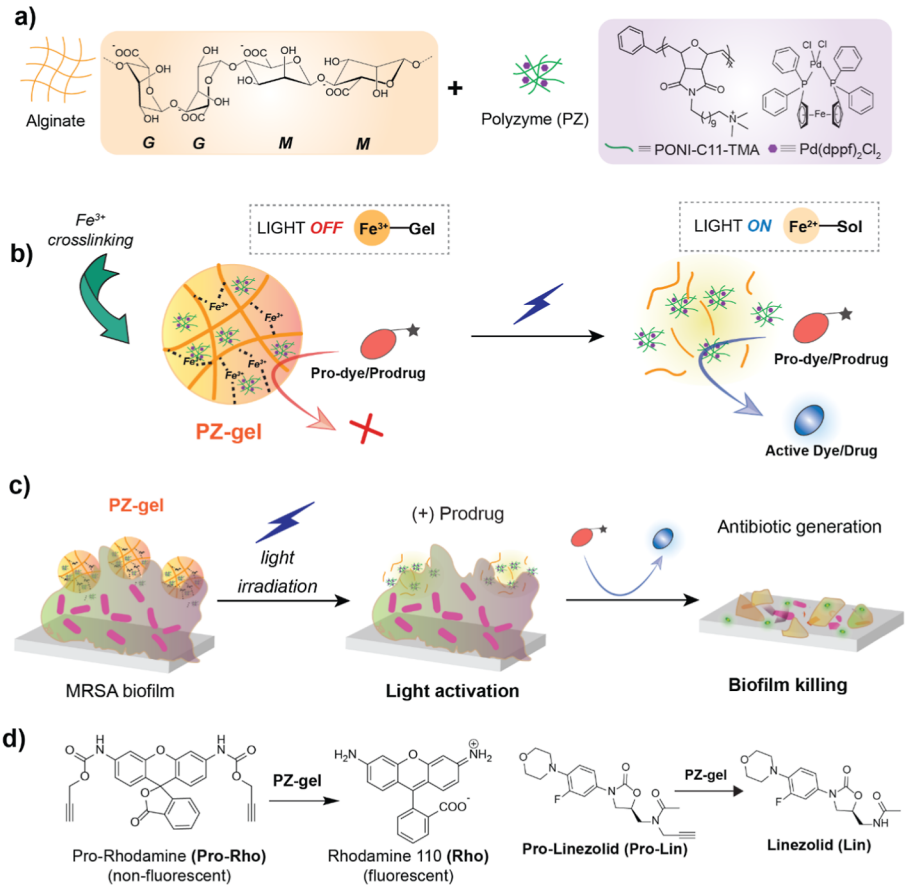

Figure 1. (a) Structures of alginate, Pd catalyst, and polymer. (b) Schematic representation of light-triggered "turn-on" **PZ-gel** dissolution and bioorthogonal activation. (c) Schematic representation of bioorthogonal activation of a pro-antibiotic with **PZ-gel** in light for biofilm reduction. (d) Pro-dye/dye (**Pro-Rho**/**Rho**) and pro-antibiotic/antibiotic (**Pro-Lin**/**Lin**) used in studies.

these nanocatalysts can be engineered for targeted localization in diseased biological environments, facilitating their use in biomedical applications.[19]

Bacterial infections, especially those caused by multidrug-resistant (MDR) bacterial strains, are an urgent and ever-growing threat to global health.[20] Additionally, bacteria have the ability to form biofilms consisting of a 3-D matrix of extracellular polymeric substances encasing the bacteria. This biofilm architecture hinders the effective penetration of conventional antibiotics, resulting in prolonged bacterial survival and increased resistance.[21,22] Consequently, biofilm-associated infections require significantly higher doses of antibiotics compared to infections caused by planktonic bacteria.[23] The complexity of biofilms, driven further by resistant gene transfer, diverse phenotypes, and persister cells[24,25] highlights their refractory nature and underscores the urgent need for alternative effective treatment regimens.

Prodrug strategies have been employed for enhancing the efficacy of antibiotics while minimizing side effects, improving the treatment of bacterial biofilms.[26] Conventional prodrug strategies rely on endogenous enzymes for activation,[27] while bioorthogonal catalysis employs mechanisms that endogenous enzymes cannot access, offering an alternative approach for prodrug activation.[28,29] Recent efforts utilizing transition-metal catalyst (TMC)-based bioorthogonal nanozymes to activate antibiotic prodrugs have shown potential in treating bacterial infections.[29] Bioorthogonal activation of pro-antibiotics of ciprofloxacin[17,30] and vancomycin[31,32] has been reported to effectively target bacterial biofilms and intracellular infections.

Although bioorthogonal nanozymes allow placement of TMCs in complex biological environments, they often lack precision in controlling temporal and spatial aspects of the bioorthogonal catalytic reactions. Spatiotemporal control of bioorthogonal nanozymes is a key strategy for achieving targeted "turn-on" therapy while minimizing off-target effects.[11,33,34] Orthotopic implantation of gold NPs in polymeric resins[35] and Cu complex in mesoporous silica[36] have been employed to localize catalysts at tumor sites and generate chemotherapeutics. Similarly, strategies such as ligand targeting, biomimetic targeting, and exploiting overexpressed enzymes, GSH levels, and pH variations in diseased tissues compared to healthy cells are common ways of targeting bioorthogonal nanozymes.[37]

External triggers such as UV and NIR light,[38−40] ultrasound,[41] and magnetic field[42] have proven effective in precise manipulation of bioorthogonal catalysis, enabling the on-demand generation of imaging agents and therapeutics, respectively. Visible light, in particular, is noninvasive and can be employed to release bioactive molecules as needed.[43,44]

Hydrogels, such as alginate, are generally recognized as safe, making them excellent matrices for the controlled and minimally invasive release of therapeutic agents,[45−47] particularly antimicrobials.[48] Light-triggered systems for controlled antibiotic release have been studied in the past,[44,49,50] with a growing emphasis on hydrogels as scaffolds.[51−53] These

https://doi.org/10.1021/acsami.5c02074
ACS Appl. Mater. Interfaces 2025, 17, 26361−26370

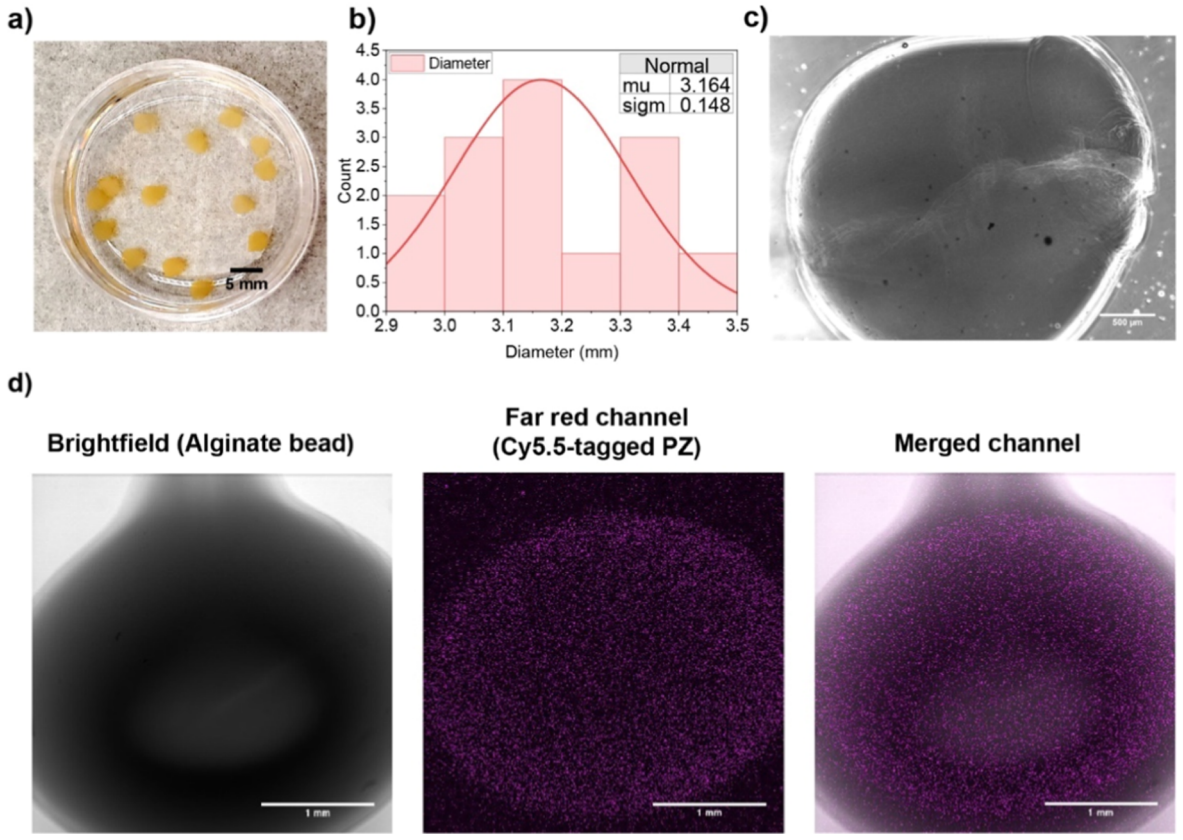

Figure 2. (a) Visual observation of **PZ-gel** dispersed in water. (Scale bar = 5 mm.) (b) Size distribution histogram of **PZ-gel** (analyzed using ImageJ software). (c) Light microscope image of a single alginate bead (scale bar = 500 μm). (d) Confocal microscopy images of a single **PZ-gel** microbead with brightfield showing an alginate bead, far-red fluorescence from the Cy5.5-tagged polymer used in PZ, and colocalization of fluorescence with an alginate bead in the merged channel showing PZ distribution within the alginate matrix (scale bar = 1 mm).

hydrogels not only facilitate controlled antibiotic release but also enhance the duration of drug presence at the infected site, especially important for chronic wound infections.[48,54,55] Alginates are commonly used in tissue engineering, wound dressing, and drug delivery applications.[46,56] Alginate, a highly water-soluble linear polymer, composed of D-mannuronate (M) and L-guluronate units (G) (Figure 1a), forms ionotropic gels when combined with divalent (Ca^{2+}, Ba^{2+}, etc.) and trivalent (Fe^{3+} and Al^{3+}) cations.[54,57] When Fe^{3+} is used as a crosslinker, sodium alginate undergoes a visible-light-activated redox-induced gel-to-sol transition.[58]

Studies have outlined methods for producing alginate hydrogels at both macro- and nanometer scales.[59] The techniques mainly cover Ca^{2+} gelation but can be easily extended to other cross-linking ions by substituting the cross-linking bath solution (typically containing $CaCl_2$) with one that contains the desired ion, like $FeCl_3{\cdot}6H_2O$. Alginate hydrogels are highly controllable in shape and size and can be tailored for specific applications. Hydrogels with smaller diameters (micro- or nanoparticles) can be generated using water-in-oil emulsions[60] or microfluidic devices.[61,62] Additionally, macroscopic alginate gels can be created through slow gelation processes[63,64] and solvent casting techniques.[65]

We hypothesized that integrating Pd-based PZs into Fe^{3+} crosslinked alginate hydrogels could enable light-responsive dissolution, thereby regulating PZ access to pro-dye and prodrug substrates for turn-on targeted therapeutic generation. Here, we present iron(III)-cross-linked alginate hydrogels loaded with PZs (**PZ-gel**) for light-triggered bioorthogonal catalysis (Figure 1). Irradiation with a ∼405 nm violet-blue light reduces Fe(III) to Fe(II), causing the gel to dissolve and exposing the PZs to propargyl-caged pro-dye/prodrug substrates. The Pd-based PZ then uncages the pro-dye and prodrug by removing the propargyl groups (Figure 1b).[4,6] This strategy enabled light-controlled activation of linezolid, a potent last-resort antibiotic,[66,67] from its inactive precursor, offering an effective treatment approach for bacterial biofilms (Figure 1c,d).

In practice, PZs were fabricated by encapsulating a palladium-based TMC into amphiphilic poly(oxanorborneneimide)-C11-trimethylamine (PONI−C11-TMA) polymer[68] through the flash nanoprecipitation (FNP) technique.[18] The PZ activity was quantified through activation of propargyl-based Rhodamine 110 pro-dye (**Pro-Rho**, Figure 1d). Once PZs were loaded in iron(III) crosslinked alginate gels (**PZ-gel**), the **PZ-gel** demonstrated catalytic activity for pro-dye activation in response to a 405 nm visible light irradiation, with minimal activation in the dark. For the treatment of multidrug-resistant *Staphylococcus aureus* (MRSA) bacterial biofilms, **PZ-gel**, when irradiated with visible light, successfully activated pro-linezolid (**Pro-Lin**, Figure 1d), showing an ∼3 log reduction of MRSA in bacterial biofilms, while no antimicrobial activity was observed for this system in the dark.

https://doi.org/10.1021/acsami.5c02074
ACS Appl. Mater. Interfaces 2025, 17, 26361−26370

RESULTS AND DISCUSSION

Fabrication of PZ-Embedded Alginate Beads. Pd-based catalysts are recognized for their effectiveness in depropargylation reactions, converting inactive precursors to useful imaging and therapeutic agents.[4,14,69] PZs with Pd TMCs were produced by rapidly mixing an aqueous stream of cationic polymer (**PONI−C11-TMA**)[66] with an organic stream of the Pd(dppf)Cl_2 catalyst through flash nanoprecipitation, as previously outlined by Huang et al.[18] When characterized, PZs were ∼25 nm in size with a surface charge of +8.4 mV (Figure S2a,b). Transmission electron microscopy and stability studies for this PZ have been performed in our previous studies.[18] The PZ activity was confirmed and quantified through **Pro-Rho** activation (Figure S3). The amount of Pd loaded in PZs was quantified with inductively coupled plasma mass spectrometry (ICP−MS, Figure S7b) with ∼0.04 mg of Pd catalyst per mg of polymer.

The PZs were then incorporated into 1% w/v sodium alginate using direct leak-proof mixing with Luer lock syringes.[70] The positively charged **PONI−C11-TMA** polymer used to fabricate the PZ was chosen to enhance electrostatic interaction with negatively charged alginate in solution and to minimize premature diffusion of PZ after gelation, as positively charged materials typically diffuse more slowly from alginate hydrogels.[56] The PZ-alginate presolution was added dropwise to a 1% v/v $FeCl_3{\cdot}6H_2O$ solution with mild stirring to allow ionic cross-linking for 15 min to form **PZ-gel** beads. The extrusion-dripping method was chosen due to its simplicity, and the ability to form uniform bead size in bulk.[56,71,72] The crosslinking solution was then removed carefully without disturbing the beads and washed with Milli-Q water twice to remove excess $FeCl_3{\cdot}6H_2O$ solution. The **PZ-gel** beads were stored in Milli-Q water for later use. **PZ-gel** beads are light yellow in color (Figure 2a) and showed an average size of 3.3 ± 0.1 mm (Figure 2b,c). We confirmed the presence and loading of PZs within the crosslinked alginate matrix using confocal microscopy and spectrophotometry, respectively. For these experiments, the Cy5.5-tagged polymer (Cy5.5-PONI-C11-TMA) (Figure S1) was used instead to form PZs and were further incorporated within 1% w/v alginate solution. In the confocal microscopy images, the brightfield channel shows a single alginate bead, and the far-red channel shows fluorescence from Cy5.5-tagged PZs. In the merged channel, the far-red fluorescence is codistributed within the alginate hydrogels, showing PZs are distributed within the cross-linked **PZ-gel** beads (Figure 2d).

We quantified the leaching of Cy5.5-tagged PZ from alginate beads during **PZ-gel** formation. Fluorescence measurements at 675/700 nm showed minimal change before and after cross-linking, indicating that minimal PZ was lost during the crosslinking process (Figure S4a). Additionally, we calculated the incorporation efficiency of PZs within **PZ-gel** by suspending 1−4 **PZ-gel** beads in phosphate-buffered solution (PBS), irradiating them with visible light for 120 min, and then measuring fluorescence of the entire **PZ-gel** solution after (Figure S4b). The amount of PZ loaded within **PZ-gel** was found to be ∼260 nM in the Cy5.5-tagged PZ/bead.

Light-Triggered Bioorthogonal Catalysis of PZ-Gel. After successful loading of PZs within alginate beads, we investigated the visible-light "turn-on" catalytic activity of **PZ-gel** through uncaging of bis-propargylated Rhodamine 110 (**Pro-Rho**) to fluorescent Rhodamine (**Rho**) (Figure 1d). **PZ-gel** (with ∼200 nM PZ) was mixed with **Pro-Rho** (10 μM) in PBS with 5 mM sodium citrate (Na-cit) as a cofactor, and light was irradiated over 2 h. The fluorescence of the solution was measured at 488/521 nm at different time points during light irradiation (Figure 3a). The **PZ-gel** in light showed increasing

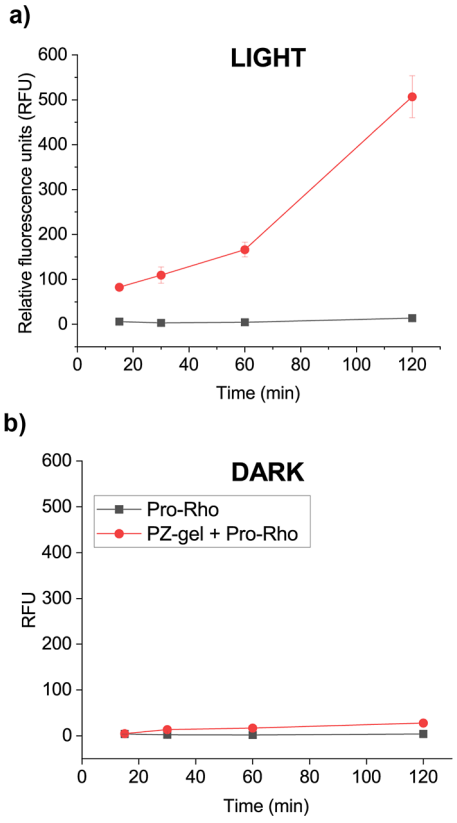

Figure 3. Catalytic activity of **PZ-gel**. Depropargylation of **Pro-Rho** to fluorescent **Rho** by **PZ-gel**. Selective catalytic activity of **PZ-gel** (200 nM PZ) monitored by **Pro-Rho** (10 μM) conversion in (a) visible light over (b) dark conditions in PBS over 2 h. All experiments were conducted with 5 mM Na-cit as a cofactor. Each data was an average of triplicates, presented as mean ± SD.

catalytic activity over time, whereas the **PZ-gel** in the dark (Figure 3b) exhibited negligible activity, establishing off-on bioorthogonal catalysis of our system. To control and enhance the degelation of **PZ-gel**, Na-cit was utilized as a cofactor as it is a known Fe^{3+} chelating agent and acts as a sacrificial carboxylate in the dissolution process.[62] The effect of different concentrations of Na-cit as a cofactor was also monitored, showing an increase in catalytic activity with higher concentrations of Na-cit (Figure S5a), likely due to faster dissolution[40,62] of **PZ-gel** with light and therefore more substrate access for the exposed PZs. In the absence of Na cit and with prolonged light exposure (Figure S5a), a slight activation of **Pro-Rho** was observed, suggesting a slow dissolution of **PZ-gel**, likely due to the reduction of Fe(III) to Fe(II). This supports the role of Na-cit as a cofactor with visible light in accelerating the **PZ-gel** dissolution process, which becomes more evident as the concentration of Na-cit increases. Interestingly, Na-cit concentrations from 0 to 5 mM did not induce significant activation of **Pro-Rho** under dark conditions (Figure S5b), indicating minimal PZ release and confirming the selective nature of the **PZ-gel** system. An optimized concentration of 5 mM Na-cit was utilized for all

https://doi.org/10.1021/acsami.5c02074
ACS Appl. Mater. Interfaces 2025, 17, 26361−26370

further experiments. The dissolution process was also monitored visually, revealing that **PZ-gel** exposed to light exhibited an increase in the turbidity of the supernatant solution, caused by gradual swelling and disintegration of **PZ-gel** over time due to the reduction of Fe (III) to Fe (II) (Figure S6).

To confirm the release of PZs from **PZ-gel** beads due to dissolution under light exposure, ^{106}Pd concentrations loaded within **PZ-gel** were measured using ICP−MS under both visible light and dark conditions. The ICP−MS data indicated an increase in Pd content by a difference of ∼4 ppb in the supernatant after 30 min of visible light irradiation compared to dark conditions (Figure S7c). This value is statistically insignificant, likely due to the short 30 min light irradiation time and the dynamic disintegration of the **PZ-gel**, which hindered capturing the full extent of the presence of Pd to account for the difference in PZ release from alginate beads. To further investigate PZ release from alginate beads, a more thorough experiment was conducted using the previously mentioned Cy5.5-tagged PZ. Fluorescence measurements were taken at various time points to track the PZ release profile under both light and dark conditions. **PZ-gel** under a 405 nm light exhibited increased PZ release with prolonged light irradiation, showing ∼13 times higher Cy5.5-tagged PZ release after 120 min compared to dark conditions (Figure S4d). The PZs released from **PZ-gel** after dissolution can then uncage **Pro-Rho**. Interestingly, a slight increment in PZ release was observed under dark conditions at extended time points. This small amount of release may be due to premature dissolution caused by the presence of Na-cit, which could gradually chelate with **PZ-gel** over time.

PZ-Gel Activation of Pro-Rho in MRSA Bacterial Biofilms. Before analyzing the catalytic activity of **PZ-gel** for biological applications, we assessed mammalian cell toxicity in 3T3 fibroblast cells (Figure S8a). We also evaluated PZ toxicity in MRSA bacterial biofilms to determine a safe concentration of 500 nM PZ (Figure S8b) in **PZ-gel** for further experiments. After confirming the light-responsive catalysis by **PZ-gel** in solution, we monitored the light-triggered **PZ-gel** catalysis within bacterial biofilms through **Pro-Rho** activation. **PZ-gel** (500 nM PZ) was incubated with a 2 day-old MRSA biofilm along with **Pro-Rho** (10 μM) with 5 mM Na-cit. After exposure to 405 nm light, **PZ-gel** showed selective activation of **Pro-Rho** in biofilms over 2 h, as shown in Figure 4a,b. Minimal activation of **PZ-gel** with **Pro-Rho** was observed in dark conditions, likely due to diffusion of **Pro-Rho** into the **PZ-gel** beads. Additionally, **Pro-Rho** was inactive only under both light and dark conditions.

Light-Based Prodrug Activation by PZ-Gel within Bacterial Biofilms. Encouraged by the light-controlled activation, we pursued the light activation of a prodrug by **PZ-gel** for eradication of MRSA bacterial biofilms. Linezolid (**Lin**, Figure 1d) is an oxazolidinone antibiotic primarily targeting Gram-positive bacteria. **Lin** is often employed as a last-resort medication in clinical treatments, especially against antibiotic-resistant strains.[44,45] Linezolid was converted into a prodrug (**Pro-Lin**) through propargylation of the secondary acylamino group (synthesis in the Experimental Section; Figures S9−S12), a modification that disrupts its interaction with the bacterial 50S ribosomal subunit[73] and reduces its antimicrobial effectiveness by more than ∼128-fold magnitude in minimum inhibitory concentration (MIC), with MIC for **Pro-Lin** = 64 μg/mL, while MIC for **Lin** = 0.25 μg/mL

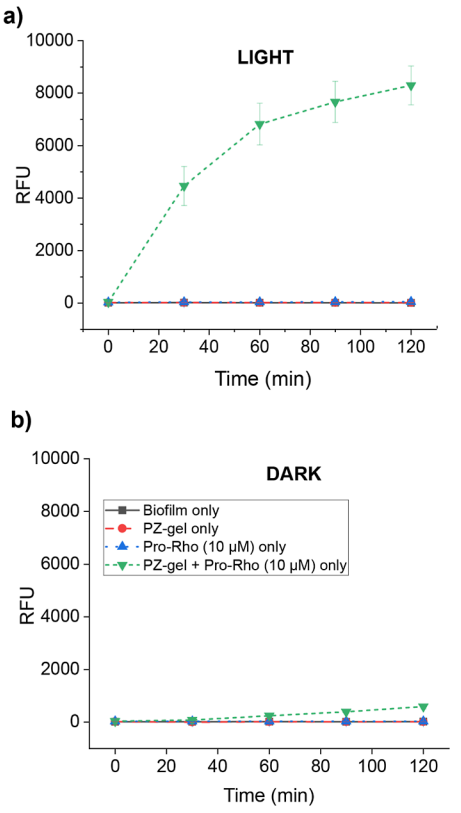

Figure 4. Catalytic activity of **PZ-gel** (500 nM PZ) through **Pro-Rho** (10 μM) activation in MRSA bacterial biofilms in the presence of (a) visible light vs (b) dark conditions. Na-cit (5 mM) was used as a cofactor. The fluorescence was measured by a plate reader (Ex/Em = 488/521 nm) and represented as an average of triplicates, presented as mean ± SD.

(Figure S13). **Pro-Lin** was inactive against MRSA biofilms as determined by the Alamar Blue assay (Figure 5a) and also the colony forming unit (CFU) count in the presence of **Pro-Lin** only (Figure 5b). Also, linezolid is the only FDA-approved drug from the oxazolidinones class of antibiotics against MRSA, whose prodrug form has not been reported before to the best of our knowledge.

To evaluate the antibiofilm efficacy by **PZ-gel** activation of **Pro-Lin**, we analyzed bacterial counts of MRSA biofilms through the CFU after treatment with **PZ-gel** and **Pro-Lin** with and without light. Biofilms treated with **Pro-Lin** only or **Lin** only served as negative and positive controls, respectively. We found that biofilms treated with both **PZ-gel** and **Pro-Lin** (128 μg/mL) in the presence of light reduced microbial cell viability (cfu/mL) by ∼3 log reduction in bacterial counts (99.9% killing) (Figure 5b). In contrast, little or no killing was observed with **PZ-gel** and prodrug in the dark. The **PZ-gel** activation of **Pro-Lin** with visible light was essentially identical to that of the free drug **Lin** only. **Pro-Lin** and **PZ-gel** demonstrated negligible toxicity on their own. These results show that **PZ-gel** provides light-activated turn-on spatiotemporal control of bioorthogonal uncaging of **Pro-Lin** with concomitant antimicrobial activity.

CONCLUSIONS

In summary, a spatiotemporal bioorthogonal system for the treatment of bacterial biofilms was generated using light-responsive Fe(III)-crosslinked alginate beads loaded with

https://doi.org/10.1021/acsami.5c02074
ACS Appl. Mater. Interfaces 2025, 17, 26361−26370

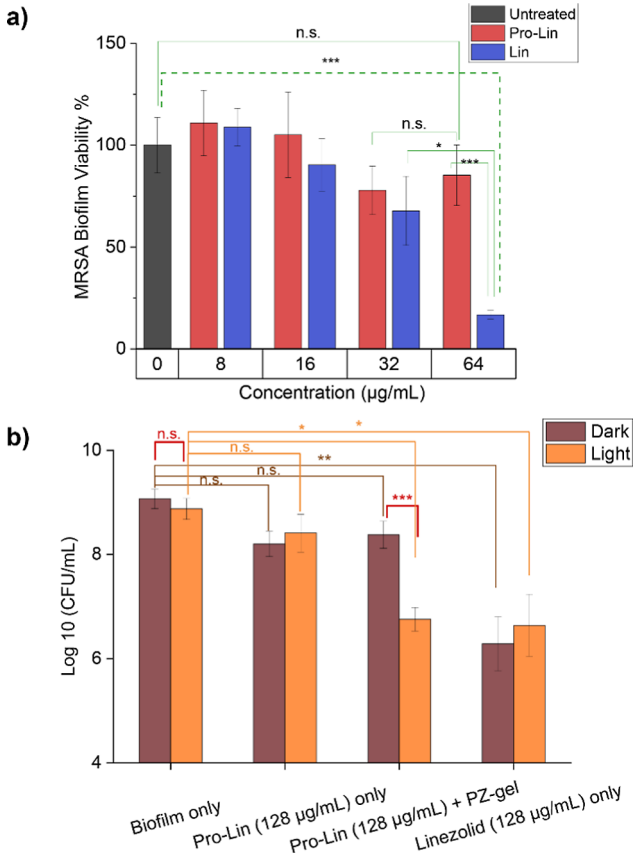

Figure 5. Light-triggered Pro-linezolid activation by **PZ-gel** in MRSA biofilms. (a) Cell viability of MRSA biofilms showing the therapeutic efficacy of **Pro-Lin** vs **Lin** by Alamar Blue assay. Efficacy in CFU reduction in MRSA biofilms by **PZ-gel** activation of (b) **Pro-Lin** (128 μg/mL).

bioorthogonal polyzymes. The PZs were distributed throughout the crosslinked beads and showed effective light-triggered catalysis within bacterial biofilms. The **PZ-gel** was selective in its activity to light with negligible activity in dark conditions and showed an effective ~3 log reduction in the bacterial count of highly resistant MRSA biofilms. Overall, this technique of combining the light-responsive properties of alginate hydrogels with the bioorthogonal catalysis of polyzymes provides a promising platform for *in situ* antibiotic generation. It offers a controllable activation mechanism with fewer side effects, including lower mammalian cell toxicity and decreased potential for resistance development. The biocompatibility and tunable configurations of iron(III)-alginate hydrogels, available in sizes ranging from nanometer to bulk gels, offer significant potential for improving the interaction and effectiveness of light-triggered bioorthogonal systems in treating biofilm infections, such as those found in chronic wounds.

EXPERIMENTAL SECTION

Polymer Synthesis. Poly(oxanorbornene-imide) (PONI−C11-TMA) was synthesized using ring opening metathesis polymerization according to previous reports.[74] The Cy5-tagged polymer (Cy5-PONI-C11-TMA) was synthesized by conjugating Cyanine5 (Cy5) NHS ester (Lumiprobe, MD) to the polymer scaffold. To an amine-functionalized polymer (5% amine), Cy5 NHS ester was added and stirred overnight in DMSO. Then, the reaction was purified by dialysis with 10,000 MWCO to afford Cy5-PONI-C11-TMA ($i\backslash j$ = 95:5) under the dark condition. The polymers were lyophilized and stored at 4 °C.

Pro-dye and Pro-drug Synthesis. *N*,*N*′-Bis-(propargyloxycarbonyl)-protected Rhodamine was synthesized by reacting commercially available Rhodamine 110 with propargyl chloroformate following a reported procedure.[75]

For prodrug synthesis: sodium hydride, NaH (35.6 mg, 0.89 mmol) dispersed as 60% in Nujol was added to an empty flask which was then evacuated and backfilled 3 times with nitrogen before chilling on ice. Ice-chilled solutions of DMF (3 mL) and propargyl bromide (80.9 mL, 1.07 mmol) were successively added. To this mixture, a chilled solution of Linezolid (**Lin**) was added dropwise over 5 min. The solution turned brown, was stirred on ice for 15 min, and then allowed to warm up to room temperature for 2.5 h. The mixture was then poured into 10 mL of saturated NH_4Cl and then washed with ethyl acetate (3 × 20 mL). The combined organic layers were then dried over $MgSO_4$. The product (R_f = 0.23, hexanes/ethyl acetate = 1:3) was then purified using flash column chromatography. **Pro-Lin** was obtained as an off-white solid (0.21 g, 64%). (^{1}H and ^{13}C NMR of **Pro-Lin** and ^{1}H of Linezolid are reported in Figures S6−S8, as well as ESI-MS in Figure S9).

Polyzyme Fabrication and PZ-Gel Formation. Polyzymes were prepared by the FNP method where an aqueous solution of the polymer and an organic solution of the catalyst was mixed through a confined impinging jet mixer. 0.6 mL of PONI−C11-TMA (1 mg/mL) was mixed with 0.6 mL of Pd catalyst (2 mg/mL) in DMSO. The outlet was connected to a 6 mL H_2O quench bath. The polyzyme solution was clear pink brown in color and was subsequently centrifuged (Amicon filter, MWCO 10 kDa) and washed with Milli-Q water five times to remove any excess catalyst. The final solution was filtered through a 0.22 μm nylon filter, and PZs were concentrated to 53.57 μM (in terms of polymer concentration) and characterized through DLS and zeta potential.

100 μL of PZ was mixed into ~1 mL of 1% w/v sodium alginate using Luer lock syringes, followed by adding the PZ-alginate presolution dropwise to a 1% v/v $FeCl_3{\cdot}6H_2O$ solution with mild stirring for 15 min to ionically crosslink and form **PZ-gel** beads. The crosslinking solution was then removed carefully without disturbing the beads and washed with Milli-Q water twice to remove excess $FeCl_3{\cdot}6H_2O$ solution. The **PZ-gel** beads were stored in Milli-Q water until further use.

Size Determination of PZ-Gel. The average size of the **PZ-gel** beads was analyzed by ImageJ analysis software. Additionally, a single **PZ-gel** bead dispersed in Milli-Q water in a round 35 mm glass bottom confocal dish was imaged through a Keyence BZ-X800 microscope at objective 4× through the brightfield channel.

Quantification of Pd/PZ and PZ Release from PZ-Gel Using ICP−MS. Pd catalysts per polymer were quantified by adding 10 μL of PZ solution (37.5 μM) to a clean 15 mL Falcon tube. 0.5 mL of fresh aqua regia was then added to the container for efficient sample digestion overnight, followed by dilution with deionized water to a total volume of 10 mL. The composition of PZ was then analyzed on a PerkinElmer NexION 300X ICP mass spectrometer. ^{106}Pd was measured under the standard mode with operating conditions as follows: nebulizer flow rate: 0.95 L/min; rf power: 1600 W; plasma Ar flow rate: 18 L/min; and dwell time: 50 ms.

Standard ME4 solutions (0, 0.2, 0.5, 1, 2, 5, 10, 20, 30, 40, 45, and 50 ppb) were prepared *via* serial dilutions for the calibration curve (Figure S7a).

For observing the release of PZ from **PZ-gel** in light vs dark conditions, **PZ-gel** beads (with PZ concentration = ~400 nM) were taken in a 48-well clear plate and dispersed in PBS with 5 mM Na-cit. One plate was exposed to visible light for 30 min, and the other plate was kept in the dark for the entire duration. The supernatant was collected from each well, transferred to a 15 mL Falcon tube as above, digested with aqua regia, and further diluted with deionized water to 10 mL The Pd content was then measured using ICP−MS.

PZ Release from PZ-Gel Using the Cy5.5-Tagged Polymer. Cy5.5 PONI−C11-TMA (see above) was utilized to fabricate Pd-loaded PZs. The Cy5.5-PZ was then incorporated into 1% alginate

https://doi.org/10.1021/acsami.5c02074
ACS Appl. Mater. Interfaces 2025, 17, 26361−26370

solution and further crosslinked using an $FeCl_3$. $6H_2O$ bath. The beads were then washed with Milli-Q water. A standard curve was generated based on the fluorescence of free Cy5.5-tagged PZ (Figure S4c). The release profile of PZ with the Cy5.5-labeled polymer was evaluated by suspending four **PZ-gel** beads in 200 μL of PBS and exposing them to light for different time intervals, up to 2 h. After each interval, 100 μL of solution was collected, and fluorescence measurements were taken to monitor the release of PZ over time.

Loading and Distribution of Cy5.5-Labeled PZs in PZ-Gel through Confocal Microscopy. Cy5.5 PONI−C11-TMA (see above) was utilized to fabricate Pd-loaded PZs. Cy5.5-PZ was then incorporated into 1% alginate solution and further crosslinked using an $FeCl_3$. $6H_2O$ bath. For loading efficiency, the crosslinker solution ($FeCl_3 \cdot 6H_2O$) was collected before and after **PZ-gel** bead formation to assess any loss of PZ due to leaching during **PZ-gel** loading and formation. The fluorescence of these solutions was then measured to determine the amount of PZ with the Cy5.5-labeled polymer that leached out during the loading process. After suspending two Cy5.5-PZ-loaded beads in 200 μL of PBS and exposing them to light irradiation for 2 h, fluorescence was measured assertively (including alginate leftover).

For confocal microscopy, after washing with Milli-Q water, the hydrated beads were then visualized in a round 35 mm glass bottom confocal dish using an A1R confocal microscope using a 4× objective in brightfield and far-red channels.

Catalytic Activity of PZ and PZ-Gel. The PZ activity was confirmed by activation of **Pro-Rho**. Briefly, **Pro-Rho** (10 μM) and PZ (1.87 μM) solutions were prepared in PBS and mixed in a black 96-well plate. The fluorescence from the conversion of **Pro-Rho** to **Rho** was monitored on a Molecular Devices M2 microplate reader (λex = 488 nm, λem = 521 nm, and cutoff = 515 nm) over time. The experiment was performed in triplicates.

For confirming the catalytic activity of **PZ-gel**, the **PZ-gel** beads were placed in a 300 μL solution of **Pro-Rho** (10 μM) in a clear 48-well plate. The plate was then irradiated with a 405 nm light for ∼2 h. At different time points during the light irradiation, 100 μL of the well solutions was taken into a black 96-well plate, and fluorescence was measured at 488/521 nm. The 100 μL was returned to the original plate for further time points. Similarly, another 24-well plate containing the **PZ-gel** and **Pro-Rho** solutions was studied under dark conditions.

Activation of Pro-Rho in Bacterial Biofilms. A single colony of methicillin-resistant *S. aureus* (IDRL-6169) was used to prepare an overnight culture in tryptic soy broth (TSB) media to obtain inoculum for culturing the mid log phase. Bacterial cells in the mid log phase were harvested and washed three times with 0.85% NaCl. The final MRSA stock solution was prepared at an optical density (O.D.) of 0.1 at 600 nm in M9 media supplemented with 10% TSB. Then, 100 μL of the seeded solution was added to each well of a 96-well microtiter plate and incubated at room temperature for 48 h. The biofilm was washed with 100 μL of PBS and then treated with **PZ-gel** and **Pro-Rho** (10 μM). Two such plates were prepared, and one was irradiated with a 405 nm light, while the other was kept covered with aluminum foil in the dark. The fluorescence in the plates were monitored by a plate reader at 488/521 nm excitation/emission, respectively, over different time points.

Bacterial Viability of PZ, Prodrug, and Drug. The mid log phase culture of MRSA (IDRL-6169) was harvested as described above. A seeding bacterial solution with an O.D. of 0.1 at 600 nm was prepared in M9 + TSB media. Then, 100 μL of the seeded solution was added to each well of a 96-well microtiter plate and incubated at room temperature for 48 h. The biofilm was washed with 100 μL of PBS and treated with different concentrations of either (i) PZ, (ii) **Pro-Lin**, or (iii) **Lin** for 24 h. After treatment, each well was washed with 100 μL of PBS and treated with Alamar Blue assay to evaluate the bacterial cell viability. The biofilm viability (%) was calculated by measuring fluorescence at 560 nm/590 nm excitation/emission, respectively.

Mammalian Cell Viability of PZ. 3T3 cells were cultured with high-glucose complete DMEM media. 10,000 Cells/well were plated in a 96-well clear plate and allowed to grow overnight. Next day, the cells were washed once with PBS and then incubated with different concentrations of PZ for 3 h. The cells were washed with PBS thrice, and then fresh media were added to the wells and incubated overnight. Next day, the cells were washed with PBS again and treated with the Alamar Blue assay to evaluate mammalian cell viability. Fluorescence was measured at the end of the experiment at 560/590 nm excitation/emission, respectively.

Activation of Pro-Lin in Bacterial Biofilms. The biofilm was grown as per the above-mentioned method, was incubated with **PZ-gel** (500 nM PZ) and **Pro-Lin** (64 or 128 μg/mL), and irradiated with a 405 nm light source for 2 h. The biofilm was further incubated for 3 h at 37 °C, followed by CFU counting of bacterial count. After treatment, the microtiter plates were wrapped with a parafilm and sonicated for 5−10 min to completely disperse the bacterial cells in the biofilm leftovers. Then, the bacterial suspension was diluted into PBS and spread into Tryptic soy agar (plates) for CFU enumeration. All the experiments were done in triplicates.

■ ASSOCIATED CONTENT

Supporting Information

The Supporting Information is available free of charge at https://pubs.acs.org/doi/10.1021/acsami.5c02074.

Preparation and activity of PZ, **PZ-gel**, polymers, pro-dye and prodrug; biological assays; and fluorescence spectra, size and charge of PZ, catalytic activity of PZ, PZ leaching, incorporation efficiency, and release profile, catalytic activity of **PZ-gel**, dissolution of **PZ-gel**, calibration curve for Pd, 3T3 viability after treatment, ^{1}H NMR of pro-Linezolid and Linezolid, ^{13}C NMR of Pro-Linezolid and Pro-Lin, and minimum inhibitory concentration (PDF)

■ AUTHOR INFORMATION

Corresponding Author

Vincent M. Rotello − *Department of Chemistry, University of Massachusetts Amherst, Amherst, Massachusetts 01003, United States;* orcid.org/0000-0002-5184-5439; Email: rotello@chem.umass.edu

Authors

Aarohi Gupta − *Department of Chemistry, University of Massachusetts Amherst, Amherst, Massachusetts 01003, United States;* orcid.org/0000-0003-1303-1159

Muhammad Aamir Hassan − *Department of Chemistry, University of Massachusetts Amherst, Amherst, Massachusetts 01003, United States*

William Ndugire − *Department of Chemistry, University of Massachusetts Amherst, Amherst, Massachusetts 01003, United States*

Jungmi Park − *Department of Chemistry, University of Massachusetts Amherst, Amherst, Massachusetts 01003, United States;* orcid.org/0000-0002-9177-4559

Sadaf Noor − *Department of Chemistry, University of Massachusetts Amherst, Amherst, Massachusetts 01003, United States; Institute of Molecular Biology and Biotechnology, Bahauddin Zakariya University, Multan 60800, Pakistan*

Harini Nagaraj − *Department of Chemistry, University of Massachusetts Amherst, Amherst, Massachusetts 01003, United States;* orcid.org/0000-0002-1615-9126

Soham Chakraborty − *Department of Chemistry, University of Massachusetts Amherst, Amherst, Massachusetts 01003, United States*

Complete contact information is available at:
https://pubs.acs.org/10.1021/acsami.5c02074

Author Contributions

The manuscript was written through contributions of all authors. All authors have given approval to the final version of the manuscript.

Funding

This research was funded by the National Institutes of Health grants EB022641 and AI134770 (Vincent M. Rotello). Muhammad Aamir Hassan and Sadaf Noor were funded by the Higher Education Commission of Pakistan. William Ndugire was funded by EB022641-S.

Notes

The authors declare no competing financial interest.

■ ABBREVIATIONS

PZ, polyzyme; PZ-gel, Polyzyme-embedded alginate hydrogel; Lin, Linezolid; Pro-Lin, Pro-Linezolid

■ REFERENCES

(1) Lozhkin, B.; Ward, T. R. Bioorthogonal Strategies for the in Vivo Synthesis or Release of Drugs. *Bioorg. Med. Chem.* **2021**, *45*, 116310.
(2) Tu, J.; Xu, M.; Franzini, R. M. Dissociative Bioorthogonal Reactions. *ChemBioChem* **2019**, *20* (13), 1615−1627.
(3) Zhang, X.; Huang, R.; Gopalakrishnan, S.; Cao-Milán, R.; Rotello, V. M. Bioorthogonal Nanozymes: Progress towards Therapeutic Applications. *Trends Chem.* **2019**, *1* (1), 90−98.
(4) Wan, X.; Zhang, Y.; Nie, Y.; Zhang, K.; Jin, Z.; Zhang, Z.; Gan, L.; Liu, X.; He, J. A. Narrative Review: Progress in Transition Metal-Mediated Bioorthogonal Catalysis for the Treatment of Solid Tumors. *Transl. Cancer Res.* **2023**, *12* (8), 2181−2196.
(5) Feng, S.; Zhang, Y.; Gao, Y.; Liu, Y.; Wang, Y.; Han, X.; Zhang, T.; Song, Y. A Gene-Editable Palladium-Based Bioorthogonal Nanoplatform Facilitates Macrophage Phagocytosis for Tumor Therapy. *Angew. Chem., Int. Ed.* **2023**, *62* (50), No. e202313968.
(6) Gao, Z.; Li, Y.; Xing, J.; Lu, Y.; Shao, Q.; Hu, J.; Zhao, S.; He, W.; Sun, B. Transition Metal Ru(II) Catalysts Immobilized Nanoreactors for Conditional Bioorthogonal Catalysis in Cells. *ACS Appl. Mater. Interfaces* **2024**, *16* (13), 15870−15878.
(7) Rubio-Ruiz, B.; Pérez-López, A. M.; Uson, L.; Ortega-Liebana, M. C.; Valero, T.; Arruebo, M.; Hueso, J. L.; Sebastian, V.; Santamaria, J.; Unciti-Broceta, A. In Cellulo Bioorthogonal Catalysis by Encapsulated AuPd Nanoalloys: Overcoming Intracellular Deactivation. *Nano Lett.* **2023**, *23* (3), 804−811.
(8) Wang, W.; Zhang, X.; Huang, R.; Hirschbiegel, C. M.; Wang, H.; Ding, Y.; Rotello, V. M. In Situ Activation of Therapeutics through Bioorthogonal Catalysis. *Adv. Drug Delivery Rev.* **2021**, *176*, 113893.
(9) Fu, Y.; Zhang, X.; Wu, L.; Wu, M.; James, T. D.; Zhang, R. *Chem. Soc. Rev.* **2025**, *54*, 201−265.
(10) Sabatino, V.; Unnikrishnan, V. B.; Bernardes, G. J. L. Transition Metal Mediated Bioorthogonal Release. *Chem Catal.* **2022**, *2* (1), 39−51.
(11) van de L'Isle, M. O. N.; Ortega-Liebana, M. C.; Unciti-Broceta, A. Transition Metal Catalysts for the Bioorthogonal Synthesis of Bioactive Agents. *Curr. Opin. Chem. Biol.* **2021**, *61*, 32−42.
(12) Liu, Z.; Guo, F.; Zhu, Y.; Qin, S.; Hou, Y.; Guo, H.; Lin, F.; Chen, P. R.; Fan, X. Bioorthogonal Photocatalytic Proximity Labeling in Primary Living Samples. *Nat. Commun.* **2024**, *15* (1), 2712.
(13) Streu, C.; Meggers, E. Ruthenium-Induced Allylcarbamate Cleavage in Living Cells. *Angew. Chem., Int. Ed.* **2006**, *45* (34), 5645−5648.
(14) Yusop, R. M.; Unciti-Broceta, A.; Johansson, E. M. V.; Sánchez-Martín, R. M.; Bradley, M. Palladium-Mediated Intracellular Chemistry. *Nat. Chem.* **2011**, *3* (3), 239−243.
(15) Tonga, G. Y.; Jeong, Y.; Duncan, B.; Mizuhara, T.; Mout, R.; Das, R.; Kim, S. T.; Yeh, Y. C.; Yan, B.; Hou, S.; Rotello, V. M. Supramolecular Regulation of Bioorthogonal Catalysis in Cells Using Nanoparticle-Embedded Transition Metal Catalysts. *Nat. Chem.* **2015**, *7* (7), 597−603.
(16) Fedeli, S.; Im, J.; Gopalakrishnan, S.; Elia, J. L.; Gupta, A.; Kim, D.; Rotello, V. M. Nanomaterial-Based Bioorthogonal Nanozymes for Biological Applications. *Chem. Soc. Rev.* **2021**, *50*, 13467−13480.
(17) Huang, R.; Li, C. H.; Cao-Milán, R.; He, L. D.; Makabenta, J. M.; Zhang, X.; Yu, E.; Rotello, V. M. Polymer-Based Bioorthogonal Nanocatalysts for the Treatment of Bacterial Biofilms. *J. Am. Chem. Soc.* **2020**, *142* (24), 10723−10729.
(18) Huang, R.; Hirschbiegel, C.-M.; Zhang, X.; Gupta, A.; Fedeli, S.; Xu, Y.; Rotello, V. M. Engineered Polymer-Supported Biorthogonal Nanocatalysts Using Flash Nanoprecipitation. *ACS Appl. Mater. Interfaces* **2022**, *14* (28), 31594−31600.
(19) Liu, Z.; Sun, M.; Zhang, W.; Ren, J.; Qu, X. Target-Specific Bioorthogonal Reactions for Precise Biomedical Applications. *Angew. Chem., Int. Ed.* **2023**, *62* (49), No. e202308396.
(20) Lancet, T. Antimicrobial resistance: an agenda for all. *Lancet* **2024**, *403* (10442), 2349.
(21) Zhao, A.; Sun, J.; Liu, Y. Understanding Bacterial Biofilms: From Definition to Treatment Strategies. *Front. Cell. Infect. Microbiol.* **2023**, *13*, 1137947.
(22) Flemming, H. C.; van Hullebusch, E. D.; Neu, T. R.; Nielsen, P. H.; Seviour, T.; Stoodley, P.; Wingender, J.; Wuertz, S. The Biofilm Matrix: Multitasking in a Shared Space. *Nat. Rev. Microbiol.* **2023**, *21* (2), 70−86.
(23) Lebeaux, D.; Ghigo, J.-M.; Beloin, C. Biofilm-Related Infections: Bridging the Gap between Clinical Management and Fundamental Aspects of Recalcitrance toward Antibiotics. *Microbiol. Mol. Biol. Rev.* **2014**, *78* (3), 510−543.
(24) Gebreyohannes, G.; Nyerere, A.; Bii, C.; Sbhatu, D. B. Challenges of Intervention, Treatment, and Antibiotic Resistance of Biofilm-Forming Microorganisms. *Heliyon* **2019**, *5* (8), No. e02192.
(25) Uruén, C.; Chopo-Escuin, G.; Tommassen, J.; Mainar-Jaime, R. C.; Arenas, J. Biofilms as Promoters of Bacterial Antibiotic Resistance and Tolerance. *Antibiotics* **2020**, *10* (1), 3.
(26) Rautio, J.; Kumpulainen, H.; Heimbach, T.; Oliyai, R.; Oh, D.; Järvinen, T.; Savolainen, J. Prodrugs: Design and Clinical Applications. *Nat. Rev. Drug Discovery* **2008**, *7* (3), 255.
(27) Larsen, E. M.; Johnson, R. J. Microbial Esterases and Ester Prodrugs: An Unlikely Marriage for Combating Antibiotic Resistance. *Drug Develop. Res.* **2019**, *80* (1), 33−47.
(28) Li, C.-H.; Huang, R.; Makabenta, J. M.; Schmidt-Malan, S.; Patel, R.; Rotello, V. M. In Situ Generation of Antibiotics Using Bioorthogonal "Nanofactories.". *Microbiol. Insights* **2021**, *14*, 117863612199712.
(29) Gupta, A.; Ndugire, W.; Liu, L.; Chakraborty, S.; Abdelaziz, M.; Rainboth, D.; Rotello, V. M. Bioorthogonal catalysis for antimicrobial therapy. *MedMat* **2024**, *1* (1), 2−5.
(30) Hardie, J.; Makabenta, J. M.; Gupta, A.; Huang, R.; Cao-Milán, R.; Goswami, R.; Zhang, X.; Abdulpurkar, P.; Farkas, M. E.; Rotello, V. M. Selective Treatment of Intracellular Bacterial Infections Using Host Cell-Targeted Bioorthogonal Nanozymes. *Mater. Horizons* **2022**, *9*, 1489.
(31) Du, Q.; Wu, X.; Bi, W.; Xing, B.; Yeow, E. K. L. Increasing Antibiotic Activity by Rapid Bioorthogonal Conjugation of Drug to Resistant Bacteria Using an Upconverted Light-Activated Photocatalyst. *J. Mater. Chem. B* **2021**, *9* (14), 3136−3142.
(32) Czuban, M.; Srinivasan, S.; Yee, N. A.; Agustin, E.; Koliszak, A.; Miller, E.; Khan, I.; Quinones, I.; Noory, H.; Motola, C.; Volkmer, R.; Di Luca, M.; Trampuz, A.; Royzen, M.; Mejia Oneto, J. M. Bio-Orthogonal Chemistry and Reloadable Biomaterial Enable Local Activation of Antibiotic Prodrugs and Enhance Treatments against Staphylococcus Aureus Infections. *ACS Cent. Sci.* **2018**, *4* (12), 1624−1632.
(33) Zhang, Y.; Lei, F.; Qian, W.; Zhang, C.; Wang, Q.; Liu, C.; Ji, H.; Liu, Z.; Wang, F. Designing intelligent bioorthogonal nanozymes:

Recent advances of stimuli-responsive catalytic systems for biomedical applications. *J. Controlled Release* **2024**, *373*, 929−951.
(34) Kumar, A.; Lee, I. S. Designer Nanoreactors for Bioorthogonal Catalysis. *Acc. Chem. Res.* **2024**, *57* (3), 413−427.
(35) Pérez-López, A. M.; Rubio-Ruiz, B.; Sebastián, V.; Hamilton, L.; Adam, C.; Bray, T. L.; Irusta, S.; Brennan, P. M.; Lloyd-Jones, G. C.; Sieger, D.; Santamaría, J.; Unciti-Broceta, A. Gold-Triggered Uncaging Chemistry in Living Systems. *Angew. Chem., Int. Ed.* **2017**, *56* (41), 12548−12552.
(36) Gao, Z.; Li, Y.; Liu, Z.; Zhang, Y.; Chen, F.; An, P.; Lu, W.; Hu, J.; You, C.; Xu, J.; Zhang, X.; Sun, B. Small-Molecule-Selective Organosilica Nanoreactors for Copper-Catalyzed Azide-Alkyne Cycloaddition Reactions in Cellular and Living Systems. *Nano Lett.* **2021**, *21* (8), 3401−3409.
(37) Zhang, W.; Zhu, J.; Ren, J.; Qu, X. Smart Bioorthogonal Nanozymes: From Rational Design to Appropriate Bioapplications. *Adv. Mater.* **2024**, *36*, 2405318.
(38) Wang, F.; Zhang, Y.; Du, Z.; Ren, J.; Qu, X. Designed Heterogeneous Palladium Catalysts for Reversible Light-Controlled Bioorthogonal Catalysis in Living Cells. *Nat. Commun.* **2018**, *9* (1), 1209.
(39) Kumar, A.; Kumar, S.; Kumari, N.; Lee, S. H.; Han, J.; Michael, I. J.; Cho, Y. K.; Lee, I. S. Plasmonically Coupled Nanoreactors for NIR-Light-Mediated Remote Stimulation of Catalysis in Living Cells. *ACS Catal.* **2019**, *9* (2), 977−990.
(40) You, Y.; Cao, F.; Zhao, Y.; Deng, Q.; Sang, Y.; Li, Y.; Dong, K.; Ren, J.; Qu, X. Near-Infrared Light Dual-Promoted Heterogeneous Copper Nanocatalyst for Highly Efficient Bioorthogonal Chemistry in Vivo. *ACS Nano* **2020**, *14* (4), 4178−4187.
(41) Xia, L.; Chen, M.; Dong, C.; Liu, F.; Huang, H.; Feng, W.; Chen, Y. Spatiotemporal Ultrasound-Driven Bioorthogonal Catalytic Therapy. *Adv. Mater.* **2023**, *35* (7), 2209179.
(42) Hoop, M.; Ribeiro, A. S.; Rösch, D.; Weinand, P.; Mendes, N.; Mushtaq, F.; Chen, X. Z.; Shen, Y.; Pujante, C. F.; Puigmartí-Luis, J.; Paredes, J.; Nelson, B. J.; Pêgo, A. P.; Pané, S. Mobile Magnetic Nanocatalysts for Bioorthogonal Targeted Cancer Therapy. *Adv. Funct. Mater.* **2018**, *28* (25), 1705920.
(43) Cios, A.; Cieplak, M.; Szymański, Ł.; Lewicka, A.; Cierniak, S.; Stankiewicz, W.; Mendrycka, M.; Lewicki, S. Effect of Different Wavelengths of Laser Irradiation on the Skin Cells. *Int. J. Mol. Sci.* **2021**, *22* (5), 2437.
(44) Kauser, A.; Parisini, E.; Suarato, G.; Castagna, R. Light-Based Anti-Biofilm and Antibacterial Strategies. *Pharmaceutics* **2023**, *15* (8), 2106.
(45) Garg, T.; Singh, O.; Arora, S.; Murthy, R. S. R. Scaffold: A Novel Carrier for Cell and Drug Delivery. *Crit. Rev. Ther. Drug Carrier Syst.* **2012**, *29* (1), 1−63.
(46) Abourehab, M. A. S.; Rajendran, R. R.; Singh, A.; Pramanik, S.; Shrivastav, P.; Ansari, M. J.; Manne, R.; Amaral, L. S.; Deepak, A. Alginate as a Promising Biopolymer in Drug Delivery and Wound Healing: A Review of the State-of-the-Art. *Int. J. Mol. Sci.* **2022**, *23* (16), 9035.
(47) Kearney, C. J.; Mooney, D. J. Macroscale Delivery Systems for Molecular and Cellular Payloads. *Nat. Mater.* **2013**, *12* (11), 1004−1017.
(48) Porter, G. C.; Schwass, D. R.; Tompkins, G. R.; Bobbala, S. K. R.; Medlicott, N. J.; Meledandri, C. J. AgNP/Alginate Nanocomposite Hydrogel for Antimicrobial and Antibiofilm Applications. *Carbohydr. Polym.* **2021**, *251*, 117017.
(49) Atkins, S.; Chueh, A.; Barwell, T.; Nunzi, J. M.; Seroude, L. Capture and Light-Induced Release of Antibiotics by an Azo Dye Polymer. *Sci. Rep.* **2020**, *10* (1), 3267.
(50) Song, Z.; Wu, Y.; Cao, Q.; Wang, H.; Wang, X.; Han, H. P. H.-R. pH-Responsive, Light-Triggered on-Demand Antibiotic Release from Functional Metal−Organic Framework for Bacterial Infection Combination Therapy. *Adv. Funct. Mater.* **2018**, *28* (23), 1800011.
(51) Deng, H.; Sun, J.; Yu, Z.; Guo, Z.; Xu, C. Low-Intensity near-Infrared Light-Triggered Spatiotemporal Antibiotics Release and Hyperthermia by Natural Polysaccharide-Based Hybrid Hydrogel for Synergistic Wound Disinfection. *Mater. Sci. Eng., C* **2021**, *118*, 111530.
(52) Shi, Y.; Truong, V. X.; Kulkarni, K.; Qu, Y.; Simon, G. P.; Boyd, R. L.; Perlmutter, P.; Lithgow, T.; Forsythe, J. S. Light-Triggered Release of Ciprofloxacin from an in Situ Forming Click Hydrogel for Antibacterial Wound Dressings. *J. Mater. Chem. B* **2015**, *3* (45), 8771−8774.
(53) Hao, Z.; Li, X.; Zhang, R.; Zhang, L. Stimuli-Responsive Hydrogels for Antibacterial Applications. *Adv. Healthcare Mater.* **2024**, *13*, No. e2400513.
(54) Pranantyo, D.; Yeo, C. K.; Wu, Y.; Fan, C.; Xu, X.; Yip, Y. S.; Vos, M. I. G.; Mahadevegowda, S. H.; Lim, P. L. K.; Yang, L.; Hammond, P. T.; Leavesley, D. I.; Tan, N. S.; Chan-Park, M. B. Hydrogel Dressings with Intrinsic Antibiofilm and Antioxidative Dual Functionalities Accelerate Infected Diabetic Wound Healing. *Nat. Commun.* **2024**, *15* (1), 954.
(55) Leppiniemi, J.; Lahtinen, P.; Paajanen, A.; Mahlberg, R.; Metsä-Kortelainen, S.; Pinomaa, T.; Pajari, H.; Vikholm-Lundin, I.; Pursula, P.; Hytönen, V. P. 3D-Printable Bioactivated Nanocellulose-Alginate Hydrogels. *ACS Appl. Mater. Interfaces* **2017**, *9* (26), 21959−21970.
(56) Lee, K. Y.; Mooney, D. J. Alginate: Properties and Biomedical Applications. *Prog. Polym. Sci.* **2012**, *37* (1), 106−126.
(57) Mollah, M. Z. I.; Zahid, H. M.; Mahal, Z.; Faruque, M. R. I.; Khandaker, M. U. The Usages and Potential Uses of Alginate for Healthcare Applications. *Front. Mol. Biosci.* **2021**, *8*, 719972.
(58) Massana Roquero, D.; Othman, A.; Melman, A.; Katz, E. Iron(iii)-Cross-Linked Alginate Hydrogels: A Critical Review. *Mater. Adv.* **2022**, *3* (4), 1849−1873.
(59) Ching, S. H.; Bansal, N.; Bhandari, B. Alginate Gel Particles−A Review of Production Techniques and Physical Properties. *Crit. Rev. Food Sci. Nutr.* **2017**, *57* (6), 1133−1152.
(60) Poncelet, D.; Babak, V.; Dulieu, C.; Picot, A. A Physico-Chemical Approach to Production of Alginate Beads by Emulsification-Internal Ionotropic Gelation. *Colloids Surf., A* **1999**, *155* (2−3), 171−176.
(61) Liu, K.; Ding, H. J.; Liu, J.; Chen, Y.; Zhao, X. Z. Shape-Controlled Production of Biodegradable Calcium Alginate Gel Microparticles Using a Novel Microfluidic Device. *Langmuir* **2006**, *22* (22), 9453−9457.
(62) Sugaya, S.; Yamada, M.; Hori, A.; Seki, M. Microfluidic Production of Single Micrometer-Sized Hydrogel Beads Utilizing Droplet Dissolution in a Polar Solvent. *Biomicrofluidics* **2013**, *7* (5), 54120.
(63) Bruchet, M.; Mendelson, N. L.; Melman, A. Photochemical Patterning of Ionically Cross-Linked Hydrogels. *Processes* **2013**, *1* (2), 153−166.
(64) Narayanan, R. P.; Melman, G.; Letourneau, N. J.; Mendelson, N. L.; Melman, A. Photodegradable Iron(III) Cross-Linked Alginate Gels. *Biomacromolecules* **2012**, *13* (8), 2465−2471.
(65) Knoop, H. E. Process for Solvent Casting a Film. US Patent 4,664,859 A May 12, 1987.
(66) Kaplan, S. L.; Afghani, B.; Lopez, P.; Wu, E.; Fleishaker, D.; Edge-Padbury, B.; Naberhuis-Stehouwer, S.; Bruss, J. B. Linezolid for the Treatment of Methicillin-Resistant Staphylococcus Aureus Infections in Children. *Pediatr. Infect. Dis. J.* **2003**, *22* (9), S178−S185.
(67) Sadowy, E. Linezolid Resistance Genes and Genetic Elements Enhancing Their Dissemination in Enterococci and Streptococci. *Plasmid* **2018**, *99*, 89−98.
(68) Gupta, A.; Landis, R. F.; Li, C. H.; Schnurr, M.; Das, R.; Lee, Y. W.; Yazdani, M.; Liu, Y.; Kozlova, A.; Rotello, V. M. Engineered Polymer Nanoparticles with Unprecedented Antimicrobial Efficacy and Therapeutic Indices against Multidrug-Resistant Bacteria and Biofilms. *J. Am. Chem. Soc.* **2018**, *140* (38), 12137−12143.
(69) Gupta, A.; Huang, R.; Rotello, V. M. Nanozymes for Emerging Therapy. In *Biomedical Nanozymes: From Diagnostics to Therapeutics*; Springer: Singapore, 2023; pp 199−299..
(70) Kearney, C. J.; Skaat, H.; Kennedy, S. M.; Hu, J.; Darnell, M.; Raimondo, T. M.; Mooney, D. J. Switchable Release of Entrapped

https://doi.org/10.1021/acsami.5c02074
ACS Appl. Mater. Interfaces 2025, 17, 26361−26370

Nanoparticles from Alginate Hydrogels. *Adv. Healthcare Mater.* **2015**, *4* (11), 1634−1639.
(71) Churio, O.; Pizarro, F.; Valenzuela, C. Preparation and Characterization of Iron-Alginate Beads with Some Types of Iron Used in Supplementation and Fortification Strategies. *Food Hydrocoll* **2018**, *74*, 1−10.
(72) Liu, G.; Zhou, H.; Wu, H.; Chen, R.; Guo, S. Preparation of Alginate Hydrogels through Solution Extrusion and the Release Behavior of Different Drugs. *J. Biomater. Sci. Polym. Ed.* **2016**, *27* (18), 1808−1823.
(73) Hashemian, S. M. R.; Farhadi, T.; Ganjparvar, M. Linezolid: A Review of Its Properties, Function, and Use in Critical Care. *Drug Des., Dev. Ther.* **2018**, *12*, 1759−1767.
(74) Makabenta, J. M. V.; Nabawy, A.; Chattopadhyay, A. N.; Park, J.; Li, C. H.; Goswami, R.; Luther, D. C.; Huang, R.; Hassan, M. A.; Rotello, V. M. Antimicrobial-Loaded Biodegradable Nanoemulsions for Efficient Clearance of Intracellular Pathogens in Bacterial Peritonitis. *Biomaterials* **2023**, *302*, 122344.
(75) Weiss, J. T.; Dawson, J. C.; Macleod, K. G.; Rybski, W.; Fraser, C.; Torres-Sánchez, C.; Patton, E. E.; Bradley, M.; Carragher, N. O.; Unciti-Broceta, A. Extracellular Palladium-Catalysed Dealkylation of 5-Fluoro-1-Propargyl-Uracil as a Bioorthogonally Activated Prodrug Approach. *Nat. Commun.* **2014**, *5*, 3277.

https://doi.org/10.1021/acsami.5c02074
ACS Appl. Mater. Interfaces 2025, 17, 26361−26370